Application of Two-Dimensional Velocity Profile to Three-Dimensional Boundary-Layer Flow

Tsze C. Tai*
David Taylor Naval Ship Research and Development Center, Bethesda, Maryland

The problem of excessive resultant velocity by using a two-dimensional profile for the streamwise flow in three dimensions is addressed. To be consistent with the physics of the boundary layer, it is proposed that the two-dimensional profile be applied to the resultant flow instead of the streamwise flow. An integral boundary-layer procedure based on the new velocity profile for theoretically determining the vortex-type flow separation is developed. The procedure is applicable to cases with large crossflows. The calculated theoretical results are compared with those obtained using the previous method, which is based on the power-law profile as applied to the streamwise flow, as well as with the available experimental data.

Nomenclature

a,b = major and minor axes of an ellipsoid
C_E = entrainment coefficient, defined in Eq. (10)
C_f = skin friction coefficient
f = local body radial distance from the centerline
H = shape factor, $=\delta^*/\theta$
h = $(H-1)/2$
h_1,h_2 = metric coefficients for coordinates ξ,η
K_1,K_2 = curvature parameters, $=\frac{1}{h_1h_2}\frac{\partial h_1}{\partial \eta}$ and $\frac{1}{h_1h_2}\frac{\partial h_2}{\partial \xi}$, respectively
M = Mach number
P = static pressure
Re = Reynolds number, $=\rho V_\infty a/\mu$
S = distance along a streamline
U = velocity at the edge of a boundary layer
u,v = velocity components in streamwise coordinates
V = resultant velocity
V_∞ = freestream velocity
$\bar{v}$ = circumferential velocity
x,ϕ = body-oriented orthogonal coordinates
$\bar{x}$ = distance along body centerline
z = ζ/δ
α = angle of attack
β = wall shear angle between external inviscid streamline and corresponding limiting streamline
γ = ratio of specific heats
δ = boundary-layer thickness
δ^* = boundary-layer displacement thickness, $=\int_0^\delta [1-(V/U)]\,d\zeta$
δ_1 = streamwise displacement thickness, $=\int_0^\delta [1-(u/U)]\,d\zeta$
δ_2 = crosswise displacement thickness, $=\int_0^\delta [1-(v/U)]\,d\zeta$
ϵ = eddy viscosity
Θ = boundary-layer momentum thickness, $=\int_0^\delta [1-(V/U)]\,(V/U)d\zeta$
Θ_{11} = streamwise momentum thickness, $=\int_0^\delta [1-(u/U)]\,(u/U)d\zeta$
$\Theta_{12},\Theta_{21},\Theta_{22}$ = crosswise momentum thickness, $=\int_0^\delta [1-(u/U)]\,(v/U)d\zeta$, $\int_0^\delta -(uv/U^2)d\zeta$, and $\int_0^\delta -(v/U)^2 d\zeta$, respectively
θ = streamline angle
λ = $\tan\beta$
μ = viscosity
ξ,η,ζ = streamwise coordinates
ρ = density
τ = shearing stress

Subscripts

x,ϕ = x,ϕ directions, respectively
w = wall
∞ = freestream
1,2 = ξ,η directions, respectively

Introduction

IN the calculation of three-dimensional boundary-layer flows, the assumption is often made that the flow in the direction of the mainstream (usually the streamwise flow) corresponds to a two-dimensional boundary-layer flow. The two-dimensional velocity profiles, as well as the auxiliary relations, therefore, are directly applicable to the streamwise flow in three dimensions. By coupling with a crossflow velocity profile, the assumption has been used exclusively in developing three-dimensional boundary-layer calculation procedures based on, but not limited to, the integral approach.[1-5] The simple addition of the crosswise component is efficient to allow adequate skewness of the resultant velocity profile in three dimensions. The approximation yields reasonably good results in the case of small crossflow conditions.[2-5]

The coupling of the crossflow imposes no direct effect on the streamwise flow. As the crossflow increases, keeping the streamwise flow in the two-dimensional form may lead to a physically unrealistic resultant velocity; its magnitude in the

Presented as Paper 85-0124 at the AIAA 23rd Aerospace Sciences Meeting, Reno, NV, Jan. 14-17, 1985; received Feb. 25, 1985; revision received June 28, 1985.

*Senior Research Scientist, Aviation and Surface Effects Department. Associate Fellow AIAA.

inner boundary layer may exceed those in the outer portion of the layer because of the large contribution of the crosswise component. The assumption thus becomes invalid in cases with large crossflows.

The purpose of the present paper is to show how the two-dimensional velocity profile can be properly applied to three-dimensional flows that are consistent with the property of the boundary layer, and still benefit from the simplicity of the conventional two-dimensional form.

Analysis

Existing Procedure

The problem of excessive velocity of the resultant flow using a two-dimensional profile for the streamwise flow in the existing procedure is best illustrated by considering the simple, power-law profile for a turbulent boundary layer,

$$u/U = z^h \tag{1}$$

where $z = \zeta/\delta$. The profile is generally valid for boundary layers with favorable pressure gradients. In existing procedures, this form is applied to the streamwise flow. By adopting a crossflow profile (for example, the Mager profile[6]), the system is complete for integration. Then,

$$\frac{v}{U} = \frac{u}{U}(1-z)^2\tan\beta \tag{2}$$

where β is the wall shear angle measured with respect to the external inviscid streamline (the mainstream). The crossflow is represented by quadric variation of the streamwise flow in the direction of β, which is treated as a wall property.[6]

The resultant velocity, based on Eqs. (1) and (2) is

$$V/U = z^h[1+(1-z)^4\tan^2\beta]^{1/2} \tag{3}$$

The resultant velocity profiles and their derivatives are shown in Figs. 1 and 2 with H and β as parameters. For $H = 1.4$, which is typical for attached flow, any β angle greater than 47 deg will yield velocity values in the inner layer higher than those in the outer region. When β is greater than 35 deg, the velocity derivative will yield a minimum inside the boundary layer. Both are inconsistent with the properties of the boundary layer. As the flow proceeds downstream, the problem becomes more severe both in decreasing H and increasing β. For $H = 1.2$, β must be limited to 27 deg without occurrence of the minimum velocity derivative inside the boundary layer; see Fig. 2.

New Procedure

To be consistent with the physics of the boundary layer, it is proposed that the two-dimensional velocity profile be applied to the resultant flow instead of the streamwise flow in three dimensions. Thus, the power-law profile is written as

$$V/U = z^h \tag{4}$$

Using the same Mager crossflow profile, Eq. (2), there results

$$u/U = z^h/[1+(1-z)^4\tan^2\beta]^{1/2} \tag{5}$$

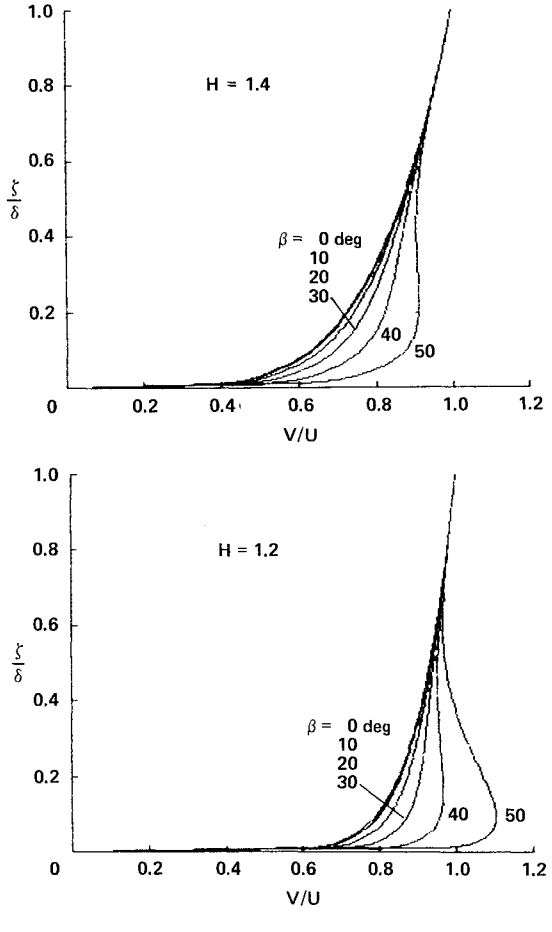

Fig. 1 Resultant velocity profiles based on power-law streamwise flow and Mager-type crossflow.

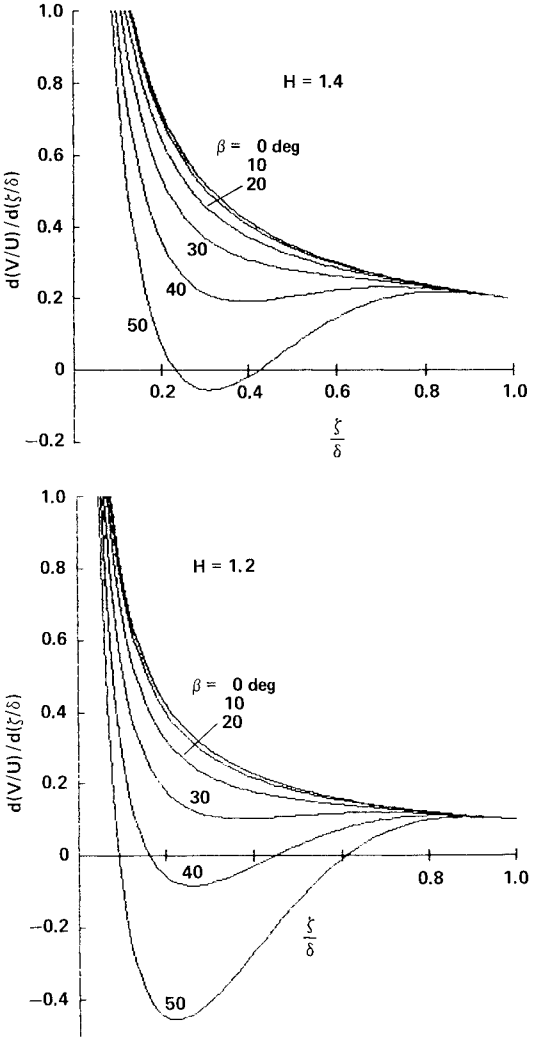

Fig. 2 Resultant velocity derivatives based on power-law streamwise flow and Mager-type crossflow.

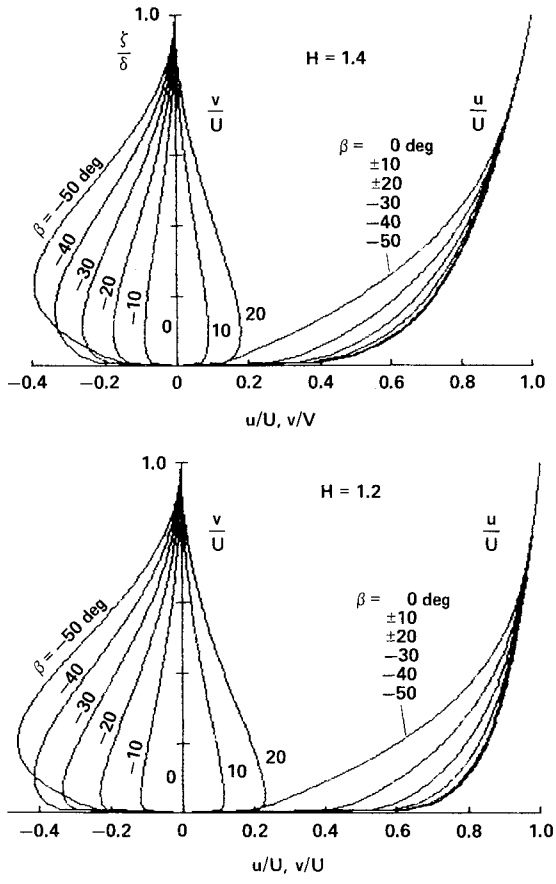

Fig. 3 New velocity profiles based on power-law resultant flow and Mager-type crossflow.

To facilitate the integration of the boundary-layer equations, Eq. (5) is approximated in the following form by retaining the first-order terms in its binomial expansion.

$$u/U = z^h[1 - \tfrac{1}{2}(1-z)^4 \tan^2\beta] \tag{6}$$

An examination of Eq. (6) reveals that any increase in crossflow leads directly to a decrease in the streamwise flow; see Fig. 3. The resultant velocity becomes skewed as a result of the crossflow increase; while its magnitude maintains the power-law variation throughout the profile.

The new profile has the advantage of automatically preventing the resultant velocity from unrealistic "swelling" near the wall. However, it may unnecessarily restrict the normal velocity growth while properly accounting for three-dimensional effects. Such a restriction is indicated by the deficient streamwise velocity profiles that may not be effectual in representing fully developed turbulent boundary layers.

For practical applications, therefore, the procedure must possess the capability of adequately accounting for three-dimensional effects without violating the physical property of the boundary layer. In view of the excellent results of the existing procedure in cases of moderate crossflow conditions, its use should be continued as long as it is valid. The new approach is developed for use where crossflow conditions are severe enough to violate the physics of the flow for the existing procedure.

Integral Solution to Three-Dimensional Turbulent Boundary Layers

In applying the new procedure to the three-dimensional integral boundary-layer method, the integral equations for an incompressible, three-dimensional, turbulent boundary layer in streamwise coordinates are:

$$\frac{1}{h_1}\frac{\partial \Theta_{11}}{\partial \xi} + \frac{1}{h_2}\frac{\partial \Theta_{12}}{\partial \eta} + \frac{2\Theta_{11}\delta_1}{Uh_1}\frac{\partial U}{\partial \xi} + (2\Theta_{21} - \delta_2)\left(\frac{1}{Uh_2}\frac{\partial U}{\partial \eta} + K_1\right) + (\Theta_{11} - \Theta_{22})K_2 = \frac{\tau_{w1}}{\rho U^2} \tag{7}$$

η momentum:

$$\frac{1}{h_1}\frac{\partial \Theta_{21}}{\partial \xi} + \frac{1}{h_2}\frac{\partial \Theta_{22}}{\partial \eta} + 2\Theta_{21}\left(\frac{1}{Uh_1}\frac{\partial U}{\partial \xi} + K_2\right) + \frac{2\Theta_{22}}{Uh_2}\frac{\partial U}{\partial \eta} - (\Theta_{11} - \Theta_{22} + \delta_1)K_1 = \frac{\tau_{w2}}{\rho U^2} \tag{8}$$

Continuity:

$$\frac{1}{h_1}\frac{\partial(\delta - \delta_1)}{\partial \xi} - \frac{1}{h_2}\frac{\partial \delta_2}{\partial \eta} + \left(K_2 + \frac{1}{Uh_1}\frac{\partial U}{\partial \xi}\right)(\delta - \delta_1) - \left(K_1 + \frac{1}{Uh_2}\frac{\partial U}{\partial \eta}\right)\delta_2 = C_E \tag{9}$$

To close the system, two-dimensional relations for the skin friction and flow entrainment are also adapted and applied to the resultant flow.

The entrainment coefficient C_E is given as a function of the shape factor H by Green et al.[7]

$$C_E = 0.025H - 0.022 \tag{10}$$

The skin friction coefficient is related to the shape factor H and the Reynolds number based on the momentum thickness Re_Θ of the resultant flow:

$$\left(\frac{C_f}{C_{f0}} + 0.5\right)\left(\frac{H}{H_0} - 0.4\right) = 0.9 \tag{11}$$

where C_{f0} and H_0 are functions of Re_Θ,

$$C_{f0} = \frac{0.01013}{\ell n Re_\Theta - 1.02} - 0.00075$$

$$H_0 = \frac{1}{1 - 6.55\sqrt{0.5C_{f0}}}$$

and Re_Θ and C_f are defined as

$$Re_\Theta = \frac{\rho U \Theta}{\mu}, \qquad C_f = \frac{\tau_w}{\frac{1}{2}\rho U^2}$$

The expressions for the curvature parameters K_1 and K_2 are derived in terms of quantities along an outer inviscid streamline[5]:

$$K_1 = \frac{1}{\gamma M^2 P}\left(-\frac{\partial P}{\partial x}\sin\theta + \frac{1}{f}\frac{\partial P}{\partial \phi}\cos\theta\right) \tag{12a}$$

$$K_2 = \frac{1}{\gamma M^2 P}\left(\frac{\partial P}{\partial x}\cos\theta + \frac{1}{f}\frac{\partial P}{\partial \phi}\sin\theta\right) + \frac{1}{U}\left(\frac{\partial U_x}{\partial x} + \frac{1}{f}\frac{\partial U_\phi}{\partial \phi} + \frac{U_x}{f}\frac{df}{dx}\right) \tag{12b}$$

Numerical Integration

Equations (7-9), with the aid of Eqs. (4-6), (10), and (11), allow solutions for three basic unknowns: the shape factor H, boundary-layer thickness δ, and the tangent of the angle between the external inviscid streamline and the corresponding limiting streamline λ. These equations are recast into the form of streamwise derivatives:

$$\frac{D\delta}{DS}=F_1 \tag{13}$$

$$\frac{D\lambda}{DS}=F_2 \tag{14}$$

$$\frac{DH}{DS}=F_3 \tag{15}$$

where $D/DS=(1/h_1)\partial/\partial\xi$, and F_1, F_2, and F_3 contain: 1) geometric properties and outer edge flow properties, 2) variables H, δ, λ, etc., and 3) crosswise derivatives of H, δ, and λ. The detailed expressions for F_1, F_2, and F_3 are presented in Ref. 8.

Application to Three-Dimensional Flow Separation

To allow direct comparison of the new approach with the existing method, the case of three-dimensional flow separation over a prolate spheriod at incidences is considered. It is assumed that the envelope of converging viscous streamlines is above, but close to, that of the converging wall-limiting streamlines. Therefore, the line of separation can be determined by the envelope of converging viscous streamlines. Thus, the boundary-layer equations are coupled with the streamline equations.[5]

$$\frac{D\phi}{DS}=\frac{\sin\theta}{f} \tag{16}$$

$$\frac{Dx}{DS}=\cos\theta \tag{17}$$

$$\frac{D\theta}{DS}=\frac{1}{\gamma M^2P}\left(\frac{\partial P}{\partial x}\sin\theta-\frac{1}{f}\frac{\partial P}{\partial\phi}\cos\theta+\frac{\partial\tau_2}{\partial\zeta}\right)-\frac{df}{dx}\frac{\sin\theta}{f} \tag{18}$$

where geometric variables are illustrated in Fig. 4. For incompressible flows, the potential flow solution[9] can be used for the pressure gradients $\partial P/\partial x$ and $\partial P/\partial\phi$ in Eq. (18). The problem is to provide proper values for the shear-stress derivative $\partial\tau_2/\partial\zeta$.

With the viscous solution in hand, the crosswise shear derivative required by Eq. (18) is obtained by differentiating Eq. (2) with the aid of the following relationships:

$$\tau_2=\epsilon\frac{\partial v}{\partial\zeta}$$

$$=\frac{\epsilon\lambda}{\delta}(1-z)\left[\frac{\partial u}{\partial z}(1-z)-2u\right] \tag{19}$$

Note that $\partial\lambda/\partial\zeta$ is zero, since λ is treated as a wall property in Mager's formulation.[6]

The eddy viscosity ϵ is correlated with the streamwise shear stress such that

$$\tau_1=\epsilon\frac{\partial u}{\partial\zeta}=\frac{\epsilon}{\delta}\frac{\partial u}{\partial z} \tag{20}$$

The value of the turbulent eddy viscosity ϵ in the crossflow is assumed to be equal to that in the streamwise flow. It is further assumed that the streamwise shear stress varies linearly across the boundary layer,

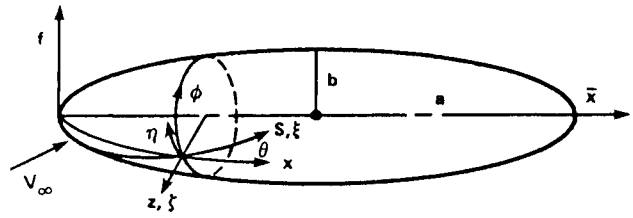

Fig. 4 Coordinate systems.

$$\tau_1=\tau_{w1}(1-z)=\tfrac{1}{2}\rho U^2C_{f1}(1-z) \tag{21}$$

With the aid of relations (19-21) along with basic profiles (2) and (6), there results

$$\frac{1}{\gamma M^2P}\frac{\partial\tau_2}{\partial\zeta}=-\frac{\lambda C_{f1}}{2\delta}z^{-2h}(1-z)\left[3(1-z)+\frac{2(1-3z)}{h(1+g)}-\frac{2z(1-z)g'}{h(1+g)^2}\right] \tag{22}$$

where

$$g=\frac{2\lambda^2z(1-z)^3}{1-\frac{1}{2}\lambda^2(1-z)^4}$$

and

$$g'=\frac{2\lambda^2(1-z)^2[1-4z-2\lambda^2z(1-z)^4]}{[1-\frac{1}{2}\lambda^2(1-z)^4]^2}$$

The difference between Eq. (22) and the previous expression given in Ref. 5 is attributed to 1) the difference in the basic profiles; 2) γM^2P, which is written as ρU^2z^{2h}; and 3) the correlation between the streamwise flow and the crossflow (which was accomplished involving the second derivative of the crossflow velocity in the previous derivation). If the λ^2 terms are neglected, g and g' would equal zero and Eq. (22) would become

$$\frac{1}{\gamma M^2P}\frac{\partial\tau_2}{\partial\zeta}=-\frac{\lambda C_{f1}}{2\delta}z^{-2h}(1-z)\left[3(1-z)+\frac{2(1-3z)}{h}\right] \tag{23}$$

A numerical experiment reveals that, for practical cases where β is smaller than 35 deg, the contribution of g and g' to the overall $\partial\tau_2/\partial\zeta$ is less than 1%. In fact, if the power-law velocity profile is applied directly to the streamwise flow, Eq. (23) would be exactly the form for the desired shear-stress derivative. Therefore, this equation is valid for both procedures.

The streamline equation, Eq. (18), is valid inside the boundary layer with variable z. In the previous calculations, the choice of the proper z layer has more or less been based on experience. A $\zeta=\delta^*$ computational layer was found to be adequate in Ref. 5. Still, such a choice lacks a mathematical basis.

To remove this assumption, Eq. (18) is integrated with respect to z so that the resulting equation describes the overall property of the boundary layer. In so doing, M^2 and $\partial\tau_2/\partial\zeta$ are treated as functions of z, while the static pressure and its derivative are kept constant across the boundary layer. Since $\gamma M^2P=\rho U^2z^{2h}$, there results

$$\frac{D\theta}{DS}=\frac{1}{\rho U^2(2-H)}\left[\frac{\partial P}{\partial x}\sin\theta-\frac{1}{f}\frac{\partial P}{\partial\phi}\cos\theta\right]+\int_0^1\frac{1}{\gamma M^2P}\frac{\partial\tau_2}{\partial\zeta}dz-\frac{df}{dx}\frac{\sin\theta}{f} \tag{24}$$

where, with the aid of Eq. (23),

$$\int_0^1 \frac{1}{\gamma M^2 P}\frac{\partial \tau_2}{\partial \zeta}dz = -\frac{\lambda C_{fl}}{2\delta}\left[\left(3+\frac{2}{h}\right)\frac{1}{2-H} - \left(6+\frac{8}{h}\right)\frac{1}{3-H}+\left(3+\frac{6}{h}\right)\frac{1}{4-H}\right] \quad (25)$$

Equations (13-17) and (24) are integrated simultaneously along a streamline. The fourth-order Runge-Kutta scheme is used in the numerical integration. To account for the crossflow derivatives, the integration is performed along at least two adjacent streamlines simultaneously. The differences in the resulting variables are then evaluated as the crossflow derivatives and immediately fed into the source terms of Eqs. (13-15). The entire procedure has been coded in BASIC language using a Hewlett-Packard 9836 desktop computer. Calculated flow patterns are instantly displayed graphically to facilitate locating the streamline convergence.

Integration Along Limiting Streamline for Case of High Angle of Attack

As the angle of attack increases, the large crossflows involved in these cases are properly represented by the new resultant velocity profile. To adequately account for the three-dimensional effect, the existing procedure is still useful as long as the crossflow angle remains moderate. When the crossflow reaches its maximum allowable value† in the old formulation, the new procedure is then immediately activated to continue the computation.

In the upstream region, however, large crossflows are often accompanied by increasing H values that may cause Eq. (24) to diverge when $H \to 2$. The problem is a numerical one and seems inherent to the power-law profile. To overcome this difficulty, integration would have to be carried out along a limiting streamline instead of a viscous streamline. The angle of a limiting streamline is

$$\theta_w = \theta + \beta \quad (26)$$

Differentiating with respect to S yields

$$\frac{D\theta_w}{DS} = \frac{D\theta}{DS} + \frac{1}{1+\lambda^2}\frac{D\lambda}{DS} \quad (27)$$

where $\lambda = \tan\beta$. The expression for $D\theta/DS$ is readily obtained by dropping the $\partial\tau_2/\partial\zeta$ term in Eq. (18). Equation (27) is to be used in place of Eq. (24) in case of a high angle of attack.

Results and Discussion

Numerical results are calculated for a prolate spheroid ($a/b = 5.91$) at a freestream $V_\infty = 147.6$ ft/s (45 m/s) and incidence $\alpha = 10$, 20, and 30 deg. Experimental results[10,11] show that the flow is turbulent in most regions. In the calculation it is assumed that the laminar and transitional flow patterns in the vicinity of the forward stagnation region are similar to those of a turbulent flow. The flow, therefore, is tripped to turbulent at $S/a = 0.10$, where the initial conditions $H = 1.46$, $\delta/a = 0.0022$, and $\lambda = 0.005$ are applied.

To establish the validity of the new approach, the results of the $\alpha = 10$ deg case are calculated completely and compared with those of the previous procedure,[5] as well as with the experimental data. For cases of $\alpha = 20$ and 30 deg, a combination of the old and new procedures was used. The previous method was employed until the crossflow exceeded its limiting value. Then the routine of the new approach was called upon to complete the computation.

Comparison of Results with the Previous Method and Experiment

Calculated results of circumferential velocity distributions in three-dimensional boundary layers are compared with experimental measurements of Meier et al.[10] for the case of a prolate spheroid at $\alpha = 10$ deg. Because the boundary-layer thickness for the circumferential flow was neither defined in the experiment nor in the present theory, comparisons were made in the form of normalized values for both velocity and distance normal to the wall. As shown in Fig. 5, the calculated profiles are in moderately good agreement with the measurements for various circumferential positions at $\bar{x}/2a = 0.73$. It is interesting that the "viscous streamwise coordinates" employed in the present method allow appearance of the mixed negative-positive circumferential velocity distributions ($\phi = 140$ deg), although the original crossflow profile in Eq. (2) does not permit change of signs inside the profile.

Results of the boundary-layer shape factor H, displacement thickness δ^*, and crossflow angle β along streamlines of $\eta = 1$ and 3 for the case of $\alpha = 10$ deg are compared with the previous theory[5] and shown in Figs. 6, 7, and 8, respectively. Comparison of the calculated results of δ^* with the available experimental data[11] is also shown.

Figures 6 and 7 show that the two approaches give slightly different values for the shape factor and the displacement thickness. Also, the skin friction values from two procedures

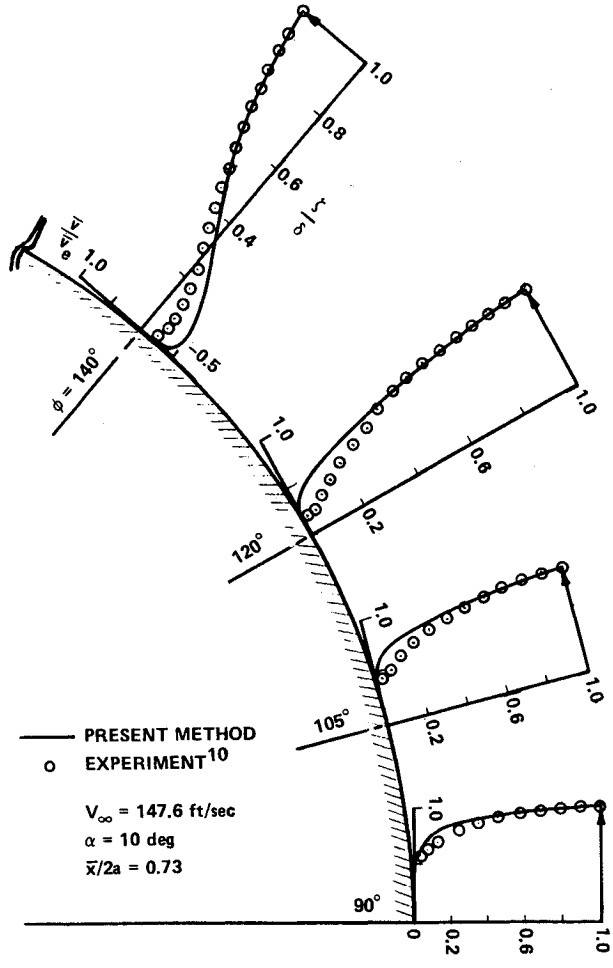

Fig. 5 Circumferential velocity distributions on a prolate spheroid at $\alpha = 10$ deg and $V_\infty = 147.6$ ft/s.

†The maximum allowable value of the crossflow in the existing procedure corresponds to the first occurrence of the minimum velocity derivative shown in Fig. 2. For $H = 1.4$ and 1.2, β must be less than 35 and 27 deg, respectively.

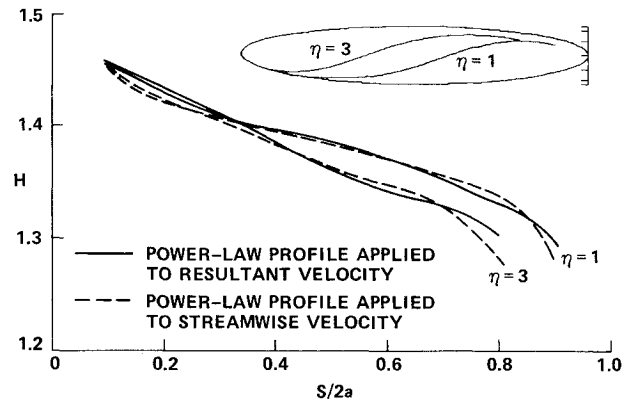

Fig. 6 Resultant boundary-layer shape factor of flow over a prolate spheroid at $\alpha = 10$ deg and $V_\infty = 147.6$ ft/s.

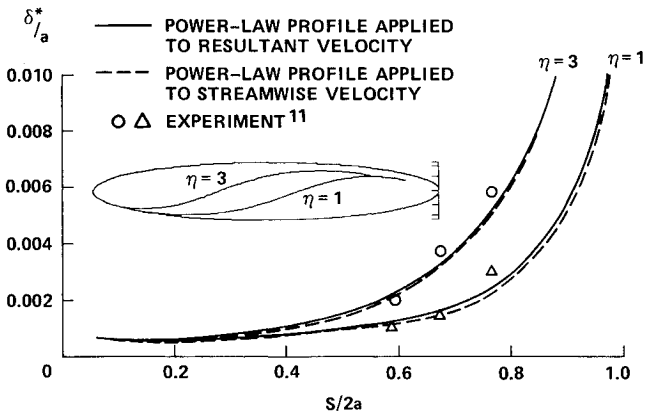

Fig. 7 Resultant boundary-layer displacement thickness of flow over a prolate spheroid at $\alpha = 10$ deg and $V_\infty = 147.6$ ft/s.

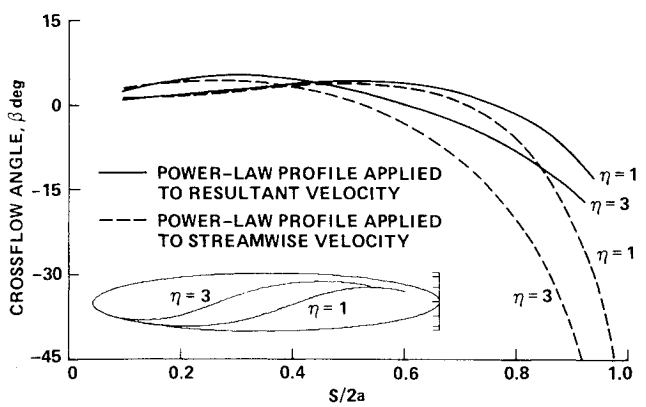

Fig. 8 Crossflow angles of flow over a prolate spheroid at $\alpha = 10$ deg and $V_\infty = 147.6$ ft/s.

lie close to each other (not shown) since the skin friction is a function of the shape factor and the momentum thickness. Comparison of δ^* values between theory and experiment is fairly good. For the crossflow angle, the results of the two approaches are comparable in the upstream region, but deviate significantly downstream where β has exceeded its limiting value in the existing method; see Fig. 8. Consequently, the location of the zero crossflow skin friction line, i.e., change of crossflow angle from positive to negative, moves closer to the separation line with the new approach. Again, the zero crossflow skin friction line is *not* a line of separation, which is consistent with experimental observations.[10,11]

The calculated overall flow pattern is shown in Fig. 9. Flow separation is detected near the rear stagnation region.

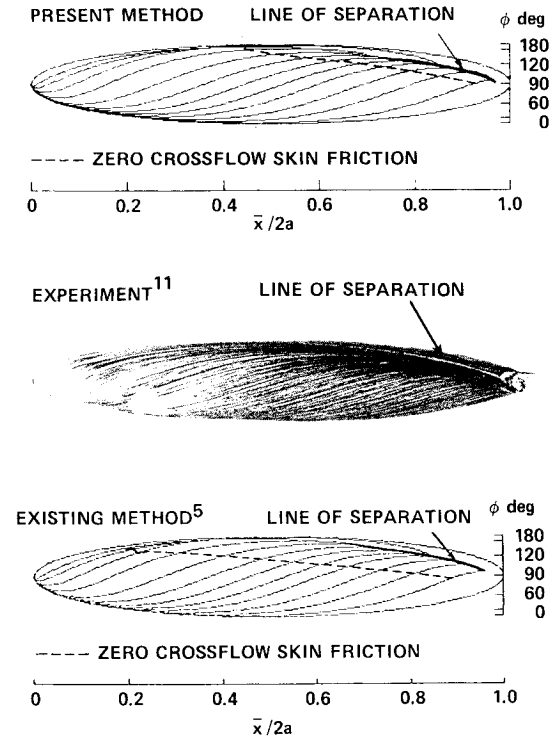

Fig. 9 Flow separation pattern on a prolate spheroid at $\alpha = 10$ deg and $V_\infty = 147.6$ ft/s.

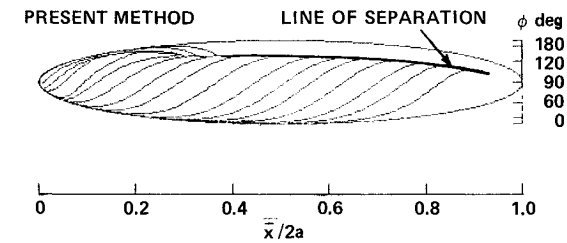

Fig. 10 Flow separation pattern on a prolate spheroid at $\alpha = 20$ deg and $V_\infty = 147.6$ ft/s.

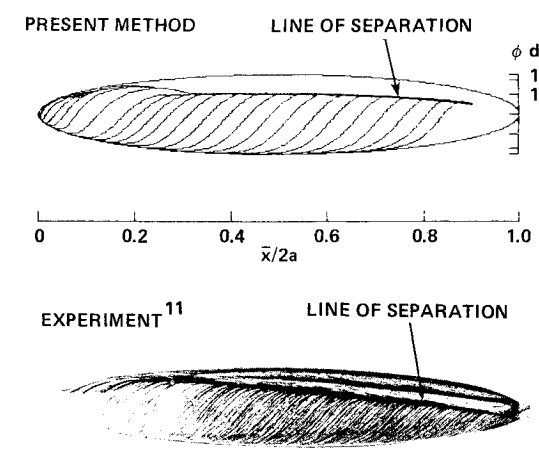

Fig. 11 Flow separation pattern on a prolate spheroid at $\alpha = 30$ deg and $V_\infty = 147.6$ ft/s.

The results are compared with those obtained with the previous technique[5] and with oil-flow visualization.[11] Excellent agreement is observed. The two procedures eventually yield almost the same results in the case of a small angle of attack. However, the location of the zero crossflow skin friction line is much closer to the line of separation using the new velocity profile. The trend is correct in view of recent data revealed by Patel and Baek.[12]

High Angle-of-Attack Cases

The results of the flow patterns at $\alpha = 20$ and 30 deg are shown in Figs. 10 and 11, respectively. The line of separation emerges further upstream creating a larger separated region in the leeside of the flow. Calculated results of the line of separation for $\alpha = 30$ deg, which were not obtainable by the old procedure without violating the physical property of the boundary layer, are compared with the available experimental data.[11] Reasonably good agreement is observed. The deviation of the theoretical result from the experimental separation line in the downstream region is believed due to the negligence of two factors: 1) the contribution of flow properties in the outer portion of the boundary layer and 2) the effect of leeside streamline "wash down." Both can be significant at large angles of attack.

As discussed previously, the power-law profile itself has its limitations of applicability. For cases of high angle of attack, perhaps a more general two-dimensional turbulent velocity profile should be considered for a more accurate representation of the three-dimensional boundary-layer flow.

Concluding Remarks

A three-dimensional integral boundary-layer approach based on the power-law profile applied to the resultant velocity is considered. The system is coupled with the streamline method for theoretically determining the vortex-type flow separation (open separation). Based on the work performed, the following conclusions are drawn:

1) The new procedure is more consistent with the physical properties of the boundary layer at large crossflow conditions and, thus, is applicable to high angle-of-attack cases.

2) In the case of small angles of attack, the new procedure yields almost identical results for the line of separation obtained using the previous method based on the power-law profile applied to the streamwise flow.

Acknowledgments

This research was sponsored by the Independent Research Program at the David Taylor Naval Ship Research and Development Center and the Naval Air Systems Command (AIR-310D, AIRTASK WR023-02). The author is grateful to the anonymous reviewer for his valuable comments and suggestions.

References

[1]Cook, J. C. and Hall, M. G., "Boundary Layers in Three Dimensions," *Progress in Aeronautical Sciences*, Vol. 2, edited by A. Ferri et al., Pergamon Press, Elmsford, NY, 1962.

[2]Smith, P. D., "An Integral Prediction Method for Three-Dimensional Compressible Turbulent Boundary Layers," Royal Aircraft Establishment, Bedford, U.K., R&M No. 3739, Dec. 1972.

[3]Cousteix, J., "Integral Method and Turbulence Models Applied to Three-Dimensional Boundary Layers," *Three-Dimensional Turbulent Boundary Layers*, edited by H. H. Fernholz and E. Krause, Springer-Verlag, Berlin, 1982, pp. 286-297.

[4]Stock, H. W. and Seibert, W., "Turbulent Boundary Layers on Three-Dimensional Configurations," *Three-Dimensional Turbulent Boundary Layers*, edited by H. H. Fernholz and E. Krause, Springer-Verlag, Berlin, 1982, pp. 366-380.

[5]Tai, T. C., "An Integral Prediction Method for Three-Dimensional Flow Separation," AIAA Paper 84-0014, Jan. 1984.

[6]Mager, A., "Generalization of Boundary Layer Momentum Integral Equations to Three-Dimensional Flows Including Those of Rotating Systems," NACA Rept. 1067, 1952.

[7]Green, J. E., Weeks, D. J., and Brooman, J. W. F., "Prediction of Turbulent Boundary-Layers and Wakes in Compressible Flow by a Lag-Entrainment Method," ARC R&M 3791, 1977.

[8]Tai, T. C., "On the Application of Two-Dimensional Velocity Profile to Three-Dimensional Boundary-Layer Flow," AIAA Paper 85-0124, Jan. 1985; also, David Taylor Naval Ship R&D Center, Bethesda, MD, Rept. DTNSRDC-85/056, June 1985.

[9]Tai, T. C., "Determination of Three-Dimensional Flow Separation by a Streamline Method," *AIAA Journal*, Vol. 19, Oct. 1981, pp. 1264-1271.

[10]Meier, H. U., Kreplin, H. P., and Vollmers, H., "Velocity Distributions in 3-D Boundary Layers and Vortex Flows Developing on an Inclined Prolate Spheroid," *Proceedings of the 6th U.S.-West Germany Data Exchange Agreement Meeting on Viscous and Interacting Flowfield Effects*, Göttingen, FRG, April 1981, pp. 202-217.

[11]Meier, H. U. and Kreplin, H. P., "Boundary Layer Separation Due to Weak and Strong Viscous-Inviscid Interaction on an Inclined Body of Revolution," *Proceedings of the 9th U.S.-West Germany Data Exchange Agreement Meeting on Viscous and Interacting Flowfield Effects*, Silver Spring, MD, May 1984, pp. 79-96.

[12]Patel, V. C. and Baek, J. H., "Boundary Layers and Separation on a Spheroid at Incidence," *AIAA Journal*, Vol. 23, Jan. 1985, pp. 55-63.